Published in final edited form as:
Pharm Res. 2010 December ; 27(12): 2528–2543. doi:10.1007/s11095-010-0256-x.

Multifunctional Peptide-PEG Intercalating Conjugates: Programmatic of Gene Delivery to the Blood-Brain Barrier

Hongwei Zhang,
Center for Drug Delivery and Nanomedicine and Department of Pharmaceutical Sciences, College of Pharmacy University of Nebraska Medical Center Omaha, Nebraska 68198, USA

Trevor Gerson,
Center for Drug Delivery and Nanomedicine and Department of Pharmaceutical Sciences, College of Pharmacy University of Nebraska Medical Center Omaha, Nebraska 68198, USA

Michelle L. Varney,
Department of Pathology and Microbiology, College of Medicine University of Nebraska Medical Center Omaha, Nebraska 68198, USA

Rakesh K. Singh, and
Department of Pathology and Microbiology, College of Medicine University of Nebraska Medical Center Omaha, Nebraska 68198, USA

Serguei V. Vinogradov
Center for Drug Delivery and Nanomedicine and Department of Pharmaceutical Sciences, College of Pharmacy University of Nebraska Medical Center Omaha, Nebraska 68198, USA

Abstract

Purpose—To enhance transfection efficacy of pDNA through the application of multifunctional peptide-PEG-*tris*-acridine conjugates (pPAC) and the formation of biodegradable core-shell polyplexes for gene delivery to the blood-brain barrier (BBB).

Methods—pPAC-mediated transfection was compositionally optimized in mouse BBB cells (bEnd.3). Cellular uptake and trafficking, and brain accumulation of pDNA was evaluated by fluorescent imaging and histochemistry. We constructed anti-MRP4 siRNA-producing vectors and evaluated the efficacy of MRP4 down-regulation of MRP4 by Western blot and qPCR, and its effect on the uptake of ^{3}H-AZT, an MRP4 substrate.

Results—A core-shell gene delivery system (GDS) was assembled from pDNA and pPAC, carrying multifunctional peptides with NLS, TAT, and brain-specific BH, or ApoE sequences, and biodegradable pLPEI polyamine. This GDS demonstrated better cellular and nuclear accumulation, and a 25-fold higher transfection efficacy in slow-dividing bEnd.3 cells compared to ExGen500. Inclusion of brain-targeting pPAC enhanced *in vivo* accumulation of functional pDNA in brain capillaries. Treatment by encapsulated anti-MRP4 siRNA-producing pDNA caused transient down-regulation of MRP4, and, after intravenous injection in Balb/c mice, enhanced AZT uptake in the brain by 230–270%.

Conclusions—The pPAC represent novel efficient components of GDS that could find various gene therapy applications, including genetic modulation of the BBB.

vinograd@unmc.edu .

Present Address: H. Zhang Gene Therapy Center, University of Massachusetts Medical School Worcester, Massachusetts 01605, USA

Keywords

ApoE peptide; AZT; blood-brain barrier; brain capillary endothelial cells; brain-homing peptide; intercalating complex; MRP4; NLS peptide; peptide-PEG conjugate; plasmid DNA; TAT peptide

INTRODUCTION

Despite the potentially higher biosafety of nonviral GDS compared to viral vectors, the transfection efficacy of nonviral vectors is far from satisfactory. During the last decade, significant progress was achieved in the area of synthetic GDS, and many important stages, roadblocks, and conditions required for efficient transfection have been identified. We now have a better understanding of the principal events accompanying intracellular transport and expression of pDNA in nuclei and can correctly design the overall program of gene delivery. A mimicking of key viral features, including transmembrane and nuclear transport, as well as the systemic targeting of GDS, was found to be very useful in the construction of prospective gene carriers (1). Numerous attempts, some of them successful and some of them not, have been made to introduce peptides carrying a nuclear localization signal (NLS) in the application to gene delivery (2). Generally speaking, only approaches that utilize NLS-related machinery would allow transfection of non-dividing or slowly-dividing cells, because pDNA transfer across the cytoplasm and through the nuclear pore was found to be one of the major efficacy-limiting obstacles (3). The second major obstacle was endosomal escape and the related transmembrane transfer of pDNA. Recently, many groups have reported the successful application of the HIV-1 Trans-Activator of Transcription (TAT) peptide with membranotropic properties for modification of GDS in order to enhance the efficacy of transmembrane transfer of pDNA (4). Hypothetically, membranotropic peptides are able to promote the bypass of the normal endosomal route and the transfer of pDNA through the nuclear pore, facilitating a direct transmembrane flip-flop (5). Among other obstacles restricting the practical utility of GDS, inefficient *in vivo* delivery and distribution of pDNA in targeted cells represent a major disadvantage in comparison with viral vectors. Although many GDSs have been decorated with PEG molecules in order to protect against binding with serum proteins and clearance by macrophages, the problem remains unsolved. Despite the fact that relatively efficient cellular targeting was achieved in many cases, the transfection efficacy was usually reversibly related to the PEG density, and a proper balance between them was difficult to find (6).

Specific targeting of the BBB has received intensive attention in view of the recent attempts to apply nano-carriers and constructs to drug delivery into the brain (7). Special emphasis was focused on the novel approaches leading to the enhancement of drug permeability across the BBB which has been severely restricted by the activity of drug efflux transporters (DET) (8). Several approaches, including genetic approaches such as RNA interference, are currently being developed in order to suppress the activity of DET in the BBB (9). Selective gene regulators potentially have more advantages than less-specific low-molecular-weight inhibitors. However, systemic pDNA or siRNA delivery to the brain faces multiple challenges and requires a stepwise programmatic approach to the design of GDS (10). Recently, we introduced a novel approach to the formulation of efficient GDS, which is based on pDNA modification with intercalating NLS-PEG-*tris*-Acr conjugates (11) and preparation of core-shell polyplexes using short biodegradable polyamines (12); these GDSs are applicable to the transfection of slowly-dividing endothelial cells and the BBB. Here, we report a general approach to pDNA modification with multifunctional peptides via pPAC and formulation of brain-targeted systemic GDS. In the first part, we describe a step-by-step optimization of these peptide formulations in order to efficiently transfect slowly-dividing mouse BCEC (bEnd.3 cells). In the second part, we demonstrate efficient brain-targeting of

these GDSs, leading to the transfection of the BBB *in vivo* and selective suppression of MRP4 DET via an RNA interference mechanism that enhanced penetration of the antiviral drug AZT into the brain.

MATERIALS AND METHODS

All solvents and reagents, except those which are specifically mentioned, were purchased from Sigma-Aldrich (St. Louis, MO) at the highest available quality grade and used without purification. Maleimide (MAL)-PEG_{5000}-*N*-hydroxysuccinimide (NHS) linker was acquired from JenKem Technology USA (Allen, TX). C-amides of peptides, HS-CAPKKKRKVA-$CONH_2$ (NLS), HSCYGRKKRRQRRR-$CONH_2$ (TAT), HS-CNAFTPDY-$CONH_2$ (BH), and HS-CGLRKLRKRLLR-$CONH_2$ (ApoE), were custom synthesized by Biomer Technology (Pleasanton, CA) and purified by semi-preparative reverse-phase HPLC. Acridine (Acr) 9-isothiocyanate was purchased from Acros Organic and re-crystallized from ethyl acetate. Biodegradable linear polyethylenimine pLPEI was synthesized as described by Zhang *et al*.(12). Both qWIZ-Luc (6.7 kb) and qWIZ-GFP (5.7 kb) plasmids were originally purchased from Gene Therapy System (San Diego, CA), propagated in *E. coli* (DH5-α), and isolated using a QIAGEN Giga Endo-free plasmid purification kit (Valencia, CA). Plasmid DNA integrity and topology were analyzed by agarose gel electrophoresis.

Synthesis and Characterization of Peptide-PEG-tris-Acridine Conjugates

All peptide-PEG_{5000}-*tris*-Acr conjugates (Fig. 1) were synthesized from the MAL-PEG_{5000}-NHS linker using a simple three-step procedure described by Zhang *et al*.(11). Unreacted maleimide moieties were quenched with cystein. Yellow pPAC was purified by semi-preparative reverse phase HPLC and lyophilized. The purified samples were analyzed for acridine content by UV spectrometry using an acridine-specific absorbance at 420 nm (Perkin-Elmer), and by amino acid analysis following acid hydrolysis (ABI Protein Analyzer, UNMC Protein Structure Core). Products with an approximately 50% degree of PEG modification by peptides were obtained (Table 1).

Cell Line Culture

Murine brain capillary endothelial cell line bEnd.3 was purchased from American Type Culture Collection (ATCC, Manassas, VA) and cultivated in Dulbecco's Modified Eagle's Medium (DMEM, Invitrogen, Carlsbad, CA) supplemented with 10% fetal bovine serum (FBS) and 2% penicillin-streptomycin in a humidified incubator in 5% CO_2 atmosphere at 37°C. Cell passages from 23 to 32 were used in transfection experiments as recommended by the supplier.

In Vitro Transfection

All transfection studies were performed in the presence of 10% FBS. Unless specifically indicated, bEnd.3 cells were seeded in a 96-well plate with an initial density of 7×10^3 cells per well 24 h prior to transfection to obtain 80% confluency upon transfection. The transfection complexes containing 0.5 μg of pDNA were added to each well and incubated for 4 h at 37°C. Then, the medium was replaced by fresh full medium, and cells were incubated for additional 40 h. When pPAC was used, pDNA was first incubated with the conjugates for 30 min at room temperature, and then mixed with ExGen500 or biodegradable pLPEI polyamine to form the final transfection complexes for an additional 30 min (Fig. 2). Luciferase expression level was determined in a Bio-Tek FLx800 microplate fluorescence reader using a Steady-Luc Firefly HTS Assay kit (Biotium, Hayward, CA). Protein content was measured by a BCA Protein Assay kit (Pierce Biotechnology, Rockford, IL). All experiments were performed in 5 parallels, and the results

were expressed as *ng* of luciferase per *mg* of protein, using a calibration curve obtained for firefly luciferase.

Fluorescent Analysis

pDNA was labeled with CX-Rhodamine by the Label IT Tracker Intracellular Nucleic Acid Localization kit/CX-Rhodamine (Mirus Bio Corp, Madison, WI) according to the manufacturer's instructions. bEnd.3 cells were seeded on 8-chamber culture slides (BD Biosciences, Bedford, MA) with an initial cell density of 4×10^4 per chamber 24 h prior to transfection. Transfection complexes containing 1.4 μg of rhodamine-labeled pDNA were added to the cells as described above. After transfection, cells were washed with PBS and fixed by 4% (w/v) paraformaldehyde for 15 min on ice. Then, a SlowFade Gold reagent with DAPI (Invitrogen, Carlsbad, CA) was applied to the cells. The slides were carefully sealed and observed under an LSM 510 laser confocal scanning microscope (LCSM, Carl Zeiss Inc., Germany).

In nuclear accumulation experiments, bEnd.3 cells were similarly treated with polyplexes; 2 h later, cells were counted, and equal amounts of cells were treated with an EZ Prep Nuclei Isolation kit (Sigma-Aldrich, St. Louis, MO) to isolate nuclei. The pure nuclear fraction was then digested using DNAzol Reagent (Invitrogen, Carlsbad, CA) to remove proteins. The fluorescence of lysates was measured in a BioTek Flx-800 multi-well plate reader at $\lambda_{ex}576/\lambda_{em}597$ nm and expressed as A.U. per 1×10^6 cells (Fig. 4B).

Green fluorescent protein-encoding vector, qWIZ-GFP, was also used to evaluate the transfection efficiency of the polymeric GDS. The transfection was conducted using a procedure identical to the one mentioned above. After 44 h of further incubation, the cells were fixed by 4% paraformaldehyde and observed by confocal microscopy at λ_{ex} 488/λ_{em} 509 nm (Fig. 4C).

Bioimaging

Balb/c mice (Charles River Laboratories) were i.v. injected in the tail vein with two doses (0.2 mL of 0.25 and 0.5 mg/mL solutions in 5% sucrose) of BH-vectorized and one dose (0.2 mL of 0.5 mg/mL solution in 5% sucrose) of nonvectorized rhodamine-labeled GDS. Animals were anesthetized by isoflurane 60 min later and observed in a Xenogen IVIS 200 system (Fig. 6).

In vivo administration of GFP pDNA was performed as above, except that mice were sacrificed on Day 3, and brains were perfused with a saline solution containing 4% paraformaldehyde, frozen, and then cut into 30 μm sections. NeutrAvidin-HRP conjugate and biotinylated anti-GFP antibody (ab69313, Abcam, Cambridge, MA) and Cy5-labeled mouse anti-CD34 antibody (BioLegend, San Diego, CA) were used for histochemistry of brain sections according to the manufacturer's instructions.

Construction of Small Interfering RNA Expression Vectors

A Gene Suppressor™ IMG-700 system (Imgenex Corp., San Diego, CA) was used in this study. Small hairpin RNA (shRNA) expression by this vector is controlled by the mammalian species-specific U6 RNA promoter. Then, shRNA is processed into active siRNA species. Three potential anti-MRP4 siRNA sequences were selected using the Imgenex siRNA Retriever program. Corresponding 54-nt oligonucleotides were then synthesized and purified by the UNMC DNA Synthesis Core Facility. Each pair of complementary oligonucleotides (100 pmol) was annealed and ligated into XhoI and XbaI sites on the vector (13). As a result, three different anti-MRP4 siRNA-producing vectors were generated and tested by their *in vitro* transfection efficacy in bEnd.3 cells. Only one

vector, which demonstrated the highest efficacy in the inhibition of MRP4 protein expression, was selected by Western blot. The complementary oligonucleotide insert used to produce this vector is shown below (the non-coding loop part is shown in italic):

5′tcgacgacgtgaacaaattcgacca*gagtactgt*ggtcgaatttgttcacgtcgttttt

3′gctgcacttgtttaagctggt*ctcatgac*accagcttaaacaagtgcagcaaaaagatc

Messenger RNA Analysis

Total cellular RNA was isolated from bEnd.3 cells using Trizol reagent (Invitrogen), and cDNA was synthesized using total RNA (5 μg), oligo(dT)$_{18}$ primer, and Superscript reverse transcriptase (RT) (Invitrogen, Carlsbad, CA). Quantitative real-time PCR (qPCR) was performed using 2 μL of a 1:100 dilution of the first-strand cDNA in FastStart DNA SYBR Green master mix with specific primers and an iCycler (Bio-Rad, Hercules, CA). Primers used were as follows: direct 5'-GGAGGAGGTACAACTTAAAG-3 ' and reverse 5 '-GTTATTCTTTAGAATGGCCC-3' (MRP4, 3547-3682, NM_001033336); and direct 5'-AGCCTCGTCCCGTAGACAAAA-3' and reverse 5'-GATGACAAGCTTCCCATTCTCG-3' (GAPDH) as a normalization standard. The fluorescence intensity of the double-stranded DNA-specific SYBR Green dye, which is proportional to the amount of PCR product, was monitored at the end of each cycle. The PCR efficiency was calculated by serial diluting the template cDNA, and the melting curve data were collected to check PCR specificity. Each cDNA sample was run in triplicate, and the corresponding sample without cDNA was included as a negative control. The mRNA levels of MRP4 gene were normalized to that of the GAPDH mRNA.

Western Blot Analysis

bEnd.3 cells were seeded and treated with anti-MRP4 pDNA in 100 mm culture dishes. After a specific time period of 4, 8, or 12 days, cells were washed four times with cold PBS and lysed in M-PER reagent (Pierce Chemicals, Rockford, IL) supplemented with a protease inhibitor cocktail (Roche Applied Sciences, Indianapolis, IN). Cellular debris was removed by centrifugation, and proteins (20 μg/lane) were separated by SDS-PAGE, electroeluted onto 0.45 mm Millipore PVDF membranes and blocked with 1% BSA in Tween-20 containing buffer. Western blot analysis was performed with rat monoclonal anti-MRP4 primary antibodies (1:500; Abcam, Cambridge, MA). After extensive washing, membranes were incubated with a rabbit polyclonal antibody to rat IgG H&L conjugated with horseradish peroxidase (1:2,000; Abcam, Cambridge, MA) for 1 h at room temperature. The membranes were developed by an enhanced chemoluminescence technique using an ECL kit (Amersham, Piscataway, NJ) and scanned using a Phosphor Imager (Molecular Dynamics, Sunnyvale, CA). Finally, membranes were stripped and re-probed with rabbit anti-β-actin antibody (1:1,000; Sigma Chemical Co. St. Louis, MO) to determine relative amounts of the loaded protein.

Brain Accumulation

Six-week-old Balb/c mice (Charles River Laboratories) were i.v. injected on Days 1, 3, and 5 with 50 μg doses of pDNA/pPAC/pLPEI formulations (20 μg of anti-MRP4 pDNA complexed with ApoE/BH-, TAT- and NLS-PEG-*tris*-Acr conjugates at the amounts 2.5 μg : 5 μg : 2.5 μg (wt) and pLPEI (20 μg). Conjugates with the BH-content of 6% and ApoE-content of 8% were used in the *in vivo* experiments. The control group was not treated with pDNA. On Day 9, each mouse was injected i.p. with 0.5 μCi of ^{3}H-AZT and sacrificed 4 h later. Brains were perfused with PBS, washed, and homogenized in Solvable Tissue Solubilizer solution (Perkin-Elmer, Boston, MA). Then, 100- aliquots were placed in the aqueous Ultima Gold scintillator solution (Sigma) and counted in a Hewlett Packard radioactivity counter.

Statistical Analysis

The significance of experimental data was determined by the Student's *t*-test (two-tailed) for *in vitro* studies and *in vivo* studies. $P<0.05$ was deemed significant. All statistical analyses were done using Prism 4 Instat software (GraphPad, San Diego, CA).

RESULTS

Peptide-PEG-*tris*-Acridine Conjugates

We synthesized all peptide-PEG_{5000}-*tris*-Acr conjugates according to the protocol used in the synthesis of NLS conjugates and published earlier (11). Initially, one of four amino groups of a propylamine dendrimer (G1.0) was modified with a bifunctional MAL-PEG_{5000}-NHS linker, and the remaining amino groups were reacted with an excess of acridine 9-isothiocyanate. The product, MAL-PEG-*tris*-Acr, was purified by gel-filtration on a Sephadex G-10 column and used directly for coupling with a two-fold molar excess of thiolated NLS, TAT, BH, or ApoE peptides. This reaction was performed overnight at 4°C under argon. The structure of peptide-PEG-tris-Acr conjugates is illustrated in Fig. 1. All non-reacted maleimide moieties were treated and capped with an excess of cystein. Finally, all conjugates were purified by semi-preparative reverse-phase HPLC on a C18 silicagel column in order to remove an excess of non-conjugated peptides and other byproducts. In general, a major wide yellow peak following the elution of free peptides was collected and concentrated. Total mass yields of solid yellow products obtained after lyophilization was 55–70%. It was practically impossible to separate unmodified PEG- and peptide-PEG-conjugates using this chromatographic method because of the wide molecular mass distribution of the PEG reagent and close elution times of both peaks. Calculated acridine content values were generally in agreement with the proposed peptide-PEG-*tris*-Acr structure (Table 1). To determine peptide content and modification rate in these conjugates, total products were hydrolyzed with acid and the amino acid content quantitatively analyzed. This analysis is also useful to confirm the amino acid sequences of peptides attached to the conjugates. In average, a nearly 50% substitution rate of the intermediate MAL-PEG-*tris*-Acr conjugate by peptides was achieved in the most efficient syntheses (Table 1). Despite numerous efforts using various conditions, we could not increase the peptide modification rate over 50%. A plausible explanation can be a partial degradation of the maleimide functionality during the two previous steps of the synthesis. Although only half of the pPAC molecules contained terminal functional peptides and could participate in the functional binding with corresponding receptors, the remaining part of non-modified PEG conjugates could serve as an additional protective shield for pDNA as was demonstrated earlier (11).

Preparation and Properties of pPAC Polyplexes

We prepared all transfecting formulations of pDNA using a two-step procedure illustrated in Fig. 2. In the first step, pDNA was complexed with the corresponding pPAC. They were shown to effectively bind pDNA because of the intercalation of acridine moieties into the DNA duplex, and the increase of steric hindrance due to the attachment of multiple PEG molecules resulted in the retention of pDNA complexes during an agarose gel electrophoresis. Since pDNA was not compacted in this procedure, no significant signal was obtained during the analysis of these complexes in aqueous media by dynamic light scattering (DLS). The pPAC-complexed pDNA could be only partially protected against degradation by nucleases (11).

The second step was an efficient compaction of pDNA complexed with pPAC by cationic polymers in order to prepare final polyplexes for transfection experiments. We used ExGen500 (linear PEI, M.w. 22,000) as a control, and recently introduced pLPEI, a biodegradable segmented linear PEI connected with disulfide bonds (M.w. 5,000) (12).

ExGen500 is considered one of most efficient currently-available transfection reagents, but this molecule is not biodegradable and relatively cytotoxic, while the pLPEI molecule is smaller and can degrade in reductive intracellular conditions. The smaller size of pLPEI can present additional advantages for the binding and compacting of peptide-PEG-decorated pDNA. ExGen500 and pLPEI were added to the complexed pDNA at N/P ratios 6 and 15, respectively, for *in vitro* experiments. For peptide-PEG-decorated pDNA (pDNA/conjugate wt ratio 2), an addition of pLPEI resulted in the formation of compact particles with a slightly higher diameter and lower zeta-potential compared to pDNA polyplex, i.e. 170±8 (PDI 0.17) and 185±6 nm (PDI 0.2), and 32 and 25 mV, respectively. The particle size of both ExGen500 and pLPEI polyplexes was similar, while the zeta-potential of ExGen500 polyplexes was slightly higher (36 mV). In conclusion, at the presented peptide-PEG-*tris*-Acr composition, pLPEI formed stable nanoparticles with core-shell architecture, containing compacted pDNA in the core decorated by PEG and peptide-PEG molecules. These peptides are exposed on the surface of polyplexes and easily accessible for binding with the corresponding cellular targets.

Transfection of bEnd.3 Cells

All pPAC conjugates demonstrated very low cytotoxicity in murine bEnd.3 cells, with IC_{50} values in the range of 0.9–1.2 mg/mL at 4 h-incubation in the presence of serum (10% FBS). ExGen500 polyplexes demonstrated a strong N/P ratio dependence in bEnd.3 cells, while polyplexes of pLPEI were generally non-toxic at all studied N/P ratios, showing a higher than 80% cell survival rate even after 24-h incubation in serum-containing media, compared to only 10% for ExGen500. Acquired data allow us to conclude that both pPAC and pLPEI are generally nontoxic in the conditions of transfection which are specific for systemic administration.

Previously, we demonstrated a strong enhancement of the *in vitro* transfection of murine bEnd.3 cells resulting from pDNA complexation with NLS-PEG-*tris*-Acr conjugates and biodegradable polyamines (11,12). Endothelial cells, including BCEC, are extremely resistant to transfection. Here, we further exploited this approach and evaluated the effects of novel TAT-, BH- and ApoE-PEG-*tris*-Acr peptide conjugates on transfection, individually or in combination, and optimized the overall composition of polyplexes. The expression of firefly luciferase-encoding pDNA was measured 48 h post-transfection in cellular medium containing 10% FBS. For NLS-PEG-tris-Acr polyplexes, only 6% of pDNA weight (DNA/NLS ratio 16:1) was sufficient to increase the transfection from 4- to 5.5-fold (Fig. 3A). The best results were obtained using PEG linkers with M.w. from 3,400 to 5,000, while PEG linker with M.w. 900 was ~25% less effective. Based on the M.w. 4,422,000 for qWIZ luc plasmid and 7,150 for NLS-PEG-*tris*-Acr conjugate, the average amount of NLS peptide required for optimal transfection performance can be calculated, giving ~38–39 NLS molecules per plasmid (ratio 8:1).

As the next step, we investigated the effect of TAT-PEG-*tris*-Acr conjugate alone (without NLS) on transfection efficacy of ExGen500 in bEnd.3 cells. This conjugate was found to be very effective as a transfection enhancer (Fig. 3B). An addition of TAT-PEG-*tris*-Acr conjugate in the amount representing only a small fraction (20%) of the pDNA weight was sufficient to increase transfection an impressive 14-fold over ExGen500, or 460 times over pDNA alone. The observed tendency was similar to the previous data on NLS-PEG-*tris*-Acr conjugates, having a bell-shaped dependence with a maximum at a DNA/TAT-conjugate weight ratio of 4. This result demonstrated that very different cellular steps of transfection have a great potential for optimization, not only nuclear translocation of pDNA. Recently, many positive effects of TAT peptide, including an enhancement of trans-membrane and nuclear translocation, and even brain delivery of nanocarriers, have been summarized (14). Thus, the presence of TAT peptide in the corona of polyplexes may serve multiple goals, the

most important of them being the enhancement of binding with endothelial cells and assistance in translocation through the cellular membrane.

When the optimal DNA/TAT-conjugate weight ratio was determined, we added various amounts of NLS-PEG-*tris*-Acr conjugate and evaluated the effect of different weight ratios of TAT/NLS conjugates on transfection efficacy of ExGen500 in bEnd.3 cells. The best transfection result was obtained at a TAT/NLS conjugate weight ratio of 2, corresponding to a DNA/NLS-conjugate ratio of 8 (Fig. 3C). Acquired data demonstrated a 64% increase over NLS-conjugate alone and a 40% increase over TAT-conjugate alone. An 18-fold enhancement over the ExGen500 polyplex and 600-fold enhancement over pDNA alone could be achieved at the optimized composition of intercalating conjugates (DNA/TAT/NLS, 8:2:1, wt).

Finally, we investigated the effect of the last component of our GDS, a brain-targeted pPAC, BH-PEG-*tris*-Acr conjugate, on transfection efficacy. Although vectorization of nanocarriers affects mostly *in vivo* accumulation, and the effect on cellular accumulation is rarely prominent *in vitro*, we decided to evaluate whether this additional modification could affect the optimized transfection efficacy of pDNA. Using ExGen500, we did not observe any statistically significant effects of this modification (data not shown). However, when the biodegradable polyamine pLPEI, a less toxic alternative to ExGen500, was used for preparation of polyplexes, we were able to see a positive, though a relatively low effect of the BH-PEG-*tris*-Acr conjugate on the transfection of bEnd.3 cells *in vitro*. As shown in Fig. 3D, pLPEI polyplexes (N/P ratio 15) were much more efficient than ExGen500 (N/P ratio 6). The summary effect of TAT and NLS conjugates on the efficacy of pLPEI polyplexes was two-fold under these conditions. When a small weight fraction of the BH conjugate was added to the optimal formulation (DNA/BH/TAT/NLS, 8:0.5:2:1, wt), no effect on transfection was observed. However, further increasing the amount of BH conjugate (DNA/BH/TAT/NLS, 8:1:2:1, wt) resulted in a 24% enhancement of the transfection of bEnd.3 cells. Altogether, it means that the overall effect of intercalating transfection enhancers may account for a nearly 800-fold enhancement of the transfection ability over naked pDNA. The weight ratio of total conjugates to pDNA was only 1:2, while the pLPEI/DNA weight ratio was approximately equal to 1.5 (N/P ratio 15). These optimized values have been used in all consequent experiments *in vitro* and *in vivo*, except where another was stated. The obtained data on efficient *in vitro* transfection of bEnd.3 cells using the pLPEI polyplexes were additionally validated in the following cell accumulation experiments.

Cell Accumulation of pDNA

We studied intracellular uptake and trafficking of rhodamine-labeled pDNA complexed with peptide-PEG-*tris*-Acr conjugates and encapsulated in pLPEI polyplexes in bEnd.3 cells by confocal microscopy. A strong synergistic effect was observed when both NLS and TAT conjugates were presented in polyplexes (Fig. 4A). The total amount of internalized pDNA (mostly located in endosomes 2 h post-transfection) was markedly increased in TAT-only and NLS+TAT samples compared to NLS-only samples. Evidently, the effect of TAT peptide on cellular accumulation of polyplexes is much more efficient than any possible effect on pDNA release from endosomes. Red fluorescence of pDNA was found to be especially abundant in the perinuclear regions and inside the nuclei in NLS+TAT samples compared to NLS-only samples.

The active role of NLS conjugates in the enhancement of nuclear accumulation of pDNA was confirmed by direct fluorescence analysis of rhodamine-labeled pDNA in whole nuclei isolated from treated bEnd.3 cells (Fig. 4B). For the treatment, we used the polyplex formulation alone, carrying a normal NLS peptide conjugate or conjugate with a mutant NLS peptide containing a single internal amino acid substitution (mNLS). We observed that

this mNLS peptide had completely lost its ability for nuclear trafficking, while normal NLS peptide increased nuclear accumulation of pDNA by 96% over non-targeted polyplexes.

To determine the effect of both specific cell targeting and nuclear targeting on transfection of bEnd.3 cells, we used polyplexes of GFP-encoding pDNA containing ApoE-conjugate or NLS+ApoE (1:1, w/w) conjugates (Fig. 4C). Confocal images obtained 16 h post-transfection of bEnd.3 cells show that the cytoplasmic and nuclear expression of GFP was significantly higher for the NLS+ApoE sample than for the NLS-only sample. Just as TAT peptide from the previous example, it is likely that the ApoE peptide further enhanced cellular binding. At the same time, the efficacy of internalization and endosomal escape of pDNA depended mostly on the positively-charged polycation forming the polyplex. Since the nuclear targeting conjugate is the same in both samples, the visible enhancement of fluorescent intensity in the NLS+ApoE sample reflected a higher copy number of pDNA initially bound to the cells.

Down-Regulation of MRP4

Murine bEnd.3 cells express high levels of ATP-dependent ABC drug efflux transporter proteins, one of which, MRP4, is responsible for the poor brain permeability of an antiviral nucleoside analog, zidovudine (AZT). Three different anti-MRP4 siRNA-producing vectors were assembled, cloned, and produced in sufficient amounts. In order to choose the best vector for MRP4 gene silencing, these anti-MRP4 pDNA were compared by their transfection efficacy using a standard ExGen500 transfection protocol in bEnd.3 cells. The level of MRP4 expression in treated cells was measured by Western blotting and real-time PCR two days post-transfection. One of three studied anti-MRP4 pDNA demonstrated an inhibitory efficacy higher than 50% and, therefore, was selected for future experiments.

In the next experiment, we determined the effect of bEnd.3 cells transfection with anti-MRP4 pDNA as a function of time, in order to identify the therapeutic window when drug treatment can be started. MRP4 RNA levels were measured by RT-qPCR analysis of total RNA samples isolated from bEnd.3 cells (Fig. 5A–B). The electrophoresis data for PCR fragments obtained after amplification of MRP4 and GAPDH sequences show stable MRP4 expression in bEnd.3 cells from passages 23–32 used in transfection experiments. Treatment by the anti-MRP4 pDNA-ExGen500 polyplex did not affect GAPDH normalization gene expression, but obviously reduced the level of MRP4 gene expression two days post-transfection (Fig. 5A). Results of the transfection with two doses of anti-MRP4 pDNA (2 and 4 μg/well) measured by RT-qPCR on Days 4, 8 and 12 are shown in Fig. 5B. Medium MRP4 inhibition (30–45%) was already evident by Day 4. Maximum down-regulation (near 60%) was obtained on Day 8 at all used doses of pDNA. Moreover, the attained inhibitory effect was observed longer after transfection, up to Day 12 (the last day of study) at a higher dose than at a lower dose of anti-MRP4 pDNA. The maximum efficacy of MRP4 gene silencing on Day 8 was then confirmed by Western blot data using β-actin as a normalization gene (Fig. 5C). Densitometry of these results demonstrated that the MRP4 protein level could be reduced to 48±7% of the level in control samples.

Finally, we evaluated how the down-regulation of MRP4 affects ^{3}H-AZT accumulation in bEnd.3 cells. Non-treated and treated bEnd.3 cells on Day 8 post-transfection were incubated with equal doses of AZT for 0.5, 1 and 2 h. Cell-associated radioactivity was measured and plotted as a function of time (Fig. 5D). The initially fast AZT uptake slowed down between 0.5 and 1 h time points in treated cells and was completely reversed in non-treated cells. AZT accumulation after 2 h incubation was 2.5-fold higher in treated cells compared to non-treated cells. One plausible explanation of the observed data is that in reality the MRP4 substrate is not AZT, but AZT monophosphate (35). Evidently, between 0.5 and 1 h after the beginning of treatment, AZT is converted into AZT monophosphate and

becomes the substrate for MRP4. In non-treated cells, AZT was pumped out of cells very quickly, while in treated cells, AZT uptake continued but slowed down slightly. In conclusion, we demonstrated *in vitro* that down-regulation of MRP4 drug efflux can significantly increase AZT drug accumulation in BCEC as the first step to the enhancement of drug permeability across the BBB.

Brain Targeting

Initially, we evaluated the efficacy of brain targeting by polyplexes with various BH and ApoE peptide densities after i.v. administration in the tail vein of Balb/c mice. Equal radioactivity doses of ^{3}H-labeled polyplexes were injected in eight groups (n=3), and brain accumulation was analyzed 1 h later, following brain perfusion (Fig. 6A). Lower peptide densities (≤4% wt) were ineffective for targeting; at least 6–8% peptide density was required to achieve a 2.5–3-fold enhancement of brain accumulation. Modification with multiple copies of both peptides demonstrated close results, although BH-vectorized formulations were statistically a little more efficient for brain delivery than ApoE-vectorized formulations at equivalent numbers of decorating peptides (3–4%, P<0.001; 4.5–6%, P<0.001; and 6–8%, P<0.05). Evidently, the difference between both peptides becomes less expressed at higher decoration degree.

In the next experiment, BH-decorated polyplexes of rhodamine-labeled pDNA were i.v. administered in Balb/c mice. Three groups of mice were injected (0.2 mL), including BH-vectorized polyplexes at 0.25 and 0.5 mg/mL (BH content: 6%) as well as a non-vectorized control. In preliminary experiments, we performed dose escalation studies of these nanoformulations, and no acute toxicity was observed up to the dose of 40 μg pDNA (100 μg polyplex) per mouse. Fluorescent body images were acquired 1 h post-injection using an IVIS-200 bioimager (Fig. 6B). The multiple copies of the brain-specific peptide on the surface were able to efficiently target decorated polyplexes to the brain. Brain accumulation was clearly dose-dependent, as shown in two sets of body pictures for animals from three treatment groups. Very low brain accumulation was observed in the case of non-vectorized polyplexes. Non-specific accumulation of BH-vectorized polyplexes was mostly localized in the lower body parts of animals, specifically the liver and bladder. No significant accumulation of polyplexes was found in the lungs. Nearly identical results were also obtained with ApoE-vectorized polyplexes *in vivo*.

To better understand brain localization of pDNA, another group of Balb/c mice was i.v. injected with non-vectorized and ApoE-decorated polyplexes (ApoE content: 8%) containing GFP-encoding pDNA (20 μg per mouse).

GFP expression was investigated in different brain sections on Day 3 post-injection using a fluorescent microscope. Figure 7A shows that pDNA was localized mostly in the brain vasculature, in the walls of blood vessels and capillaries. GFP fluorescence distribution is shown after background fluorescence compensation (Fig. 7A: b, d). Some insignificant fluorescence was also observed in brain tissue; however, this fluorescence still may be related to the background autofluorescence of the brain. We performed additional staining of brain sections with an anti-GFP antibody in order to confirm the location of GFP expression. The brown staining (DAB) is clearly visible in brain capillaries (Fig. 7A: a, c). Finally, we co-stained the vasculature in the brain samples with Cy5-labeled endothelium-specific anti-CD34 antibodies. As seen in Fig. 7B, both red (a) and green (b) fluorescence overlap in the walls of brain capillaries (d). These results demonstrate that functionally-active pDNA can be efficiently delivered into the brain vasculature by brain-specific peptide-targeted polyplexes following an i.v. administration.

Enhancement of AZT Transport in the Brain

Two groups of Balc/c mice were i.v. injected on Days 1, 3 and 5 with three doses (20 μg/mouse) of anti-MRP4 pDNA encapsulated in brain-vectorized LPEI-polyplexes containing 2.5 μg of BH/ApoE, 5.0 μg of TAT, and 2.5 μgof NLS conjugates. The control group was left untreated. On Day 9, all animals were i.p. injected with identical doses of ^{3}H-AZT. Four h post-injection, their brains were perfused, and radioactivity was measured in treated brain tissues (Fig. 8). Our results demonstrate a statistically significant increase in AZT brain permeation following anti-MRP4 treatment ($P<0.001$). In the non-treated control group, AZT uptake was equal to 0.19%ID/g. In treated groups, we observed a 3.3-fold to 3.7-fold increase of AZT uptake after treatment by ApoE- and BH-decorated polyplexes, respectively, representing 0.63 and 0.72% ID/g. Thus, summarizing all presented data, we conclude that transient down-regulation of the MRP4 DET by systemic administration of anti-MRP4 pDNA encapsulated into the pPAC-pLPEI-based GDS can be successfully used for inducing better drug permeability of the BBB.

DISCUSSION

Here we attempted to reach two major goals in the development of efficient non-viral GDS: (1) to design a novel GDS based on the current knowledge of major cellular events accompanying pDNA transport into the nucleus for more efficient transfection of slowly dividing cells, and (2) to apply the optimized GDS in order to achieve *in vivo* modulation of selected drug efflux transporters, and enhance drug permeability across the BBB. Three major advances were laid in the core of this approach: (1) application of short peptides for enhancing cell-specific targeting, trans-membrane transfer and nuclear translocation of pDNA, (2) direct modification of pDNA by intercalating peptide-PEG-*tris*-Acr conjugates, and (3) protective compaction of pDNA with biodegradable SS-polyamines.

The principal steps of non-viral transfection include the following: *in vivo* delivery, binding to the cellular membrane, internalization, endosomal escape, nuclear transport, and transgene expression. There are serious restrictions to the current efficacy of each of these steps. For example, easy degradation by nucleases requires pDNA encapsulation in protective complexes; however, an incomplete release of free pDNA from these complexes can hamper its transfection activity (15). An arrest of internalized complexes in endosomes usually results in the degradation and loss of activity of pDNA. Lipid cellular membranes create serious barriers to pDNA passage inside the cytoplasm, but even there, supercoiled pDNA molecules are too large to move unassisted in the cytoplasm and through the small nuclear pore complex which is only 22 nm in diameter (16). Or, for example, *in vivo* administration of complexed pDNA requires surface decoration with PEG to prevent binding of serum proteins and phagocytosis or increased targeting by specific vector ligands. However, a high density of PEG decoration can also render interactions with cells and internalization of pDNA complexes ineffective (17).

In order to manage many of the problems associated with non-viral GDS, we recently introduced multifunctional transfection enhancers, peptide-PEG-*tris*-Acr conjugates, which are able to bind pDNA by intercalation. Acridine derivatives are relatively nontoxic and known for their ability to pass through the BBB; their safety has also been confirmed by long-term usage of acridine-based drugs in chemotherapy (18). In the presence of an excess of chromosomal DNA in nuclei, these intercalated conjugates must be capable of releasing functionally active pDNA. Initial proof-of-concept was done through the use of NLS-PEG-*tris*-Acr conjugates in association with polyplexes (11,12). In some instances, short NLS peptides demonstrated the ability to increase efficacy of transfection and nuclear accumulation of pDNA; however, no positive effect was observed by many researchers (19). It is worth noting that mostly positive effects have been observed when pDNA was modified

with NLS peptide covalently, or via intercalation. Encapsulation of the NLS-modified pDNA with transfection reagents sometimes can abolish these positive effects, because pDNA release from these complexes became a rate-limiting step. Since biodegradable SS-polyamines allowed easier pDNA release after degradation inside the cells, they represent “reagents of choice” for the preparation of polyplexes (20,21).

The trans-membrane activity of TAT peptide is well documented, and its applications go beyond gene delivery. Potentially, modification of GDS by TAT peptide can enhance many steps of pDNA delivery, such as internalization, endosomal escape, and nuclear transport. Among the applications of TAT peptide for gene delivery, observed data are usually more consistent and positive than data on applications of NLS peptide. In our experiments, the effect of TAT modifications was generally higher than the effect of NLS modifications. TAT peptide is very efficient alone, in concert with NLS peptide, or with PEI-based polyamines, e.g. enhancing the endosomal escape of pDNA (22). An independent confirmation of the synergism in the action of TAT and NLS peptides during an *in vitro* transfection was recently obtained for DNA-binding peptide-PEG-NLS/TAT conjugates (23). Nuclear transport of pDNA may be enhanced by modification with TAT peptide because of a potential bypass of nuclear pore-related transfer (24). We observed an efficient increase of nuclear accumulation of pDNA even after treatment with polyplexes containing only TAT conjugates.

Specific cell targeting could increase cellular accumulation of pDNA and, therefore, the efficacy of all downstream events before *in nuclei* gene expression. We observed a significant transfection-enhancing effect of BCEC targeting by including conjugates of short brain-homing (BH) (25) or apolipo-protein E receptor-specific (ApoE) peptides in the designed GDS. This effect was dependent on the modification density, i.e. the number of targeting peptides attached to polyplex. We also found an obvious cumulative effect of decoration by multiple peptides on the transfection ability of modified polyplexes. Evidently, this complex system may require further optimization. One of the ways to that goal could be intracellular cleavage of PEG and BH/ApoE-PEG molecules from the surface of polyplexes, enabling better presentation of TAT- and NLS-PEG moieties, which are essential to the following pDNA delivery steps. For example, both PEG fragments can be connected to the common dendrimer-*tris*-acridine moiety via biodegradable disulfide bonds. A similar approach, including the removal of PEG decoration for better binding with the cellular membrane, was recently reported (26,27). The second optimization approach can include PEG decoration to an overall degree where no significant non-specific organ binding *in vivo* is detected and, after that, a rational selection of the best ratio of peptide components in order to obtain a maximized transfection efficacy (28,29). Summarizing presented data, we want to stress that these novel transfection enhancers (pPAC) are of general interest and can be applied to the preparation of various therapeutic gene formulations with high efficacy, including those for slowly-dividing cells resistant to transfection.

Poor drug permeability of the BBB presents a significant challenge in the chemotherapy of various CNS-related diseases. Many antiviral and anticancer nucleoside analogs, the first-line therapeutic drugs, have restricted access into the brain due to the activity of DET located on the luminal side of the brain capillaries, the BCEC composing the BBB (8,30). Rational modulation of drug permeability across the BBB by DET inhibitors is considered a promising direction in drug development. This general approach is based on the application of various inhibitor molecules (9,31), or transcriptional inhibition of protein synthesis due to an effective mRNA degradation (32,33). Currently, it is accepted that HIV-1 reservoirs in the brain are major causes of both AIDS recurrence after application of highly active antiretroviral therapy (HAART) and the development of drug-resistant viral strains. In anti-AIDS treatment, AZT is one of the major drug components of HAART. However, it was

found that less than 0.1% of AZT passing through brain capillaries with the blood accumulates in the brain. The maximum AZT concentration in the brain could not reach the effective antiviral concentration, 0.05 μg/mL, even after the injection of 5 mg/kg AZT (34). Previously, MRP4 and MRP5 DET have been identified as transporters affecting the accumulation of AZT in the brain (35). MRP4 was also the most highly expressed protein in the MRP series in BCEC. In this work, we experimentally demonstrated that inhibition of MRP4 results in a significant increase in brain accumulation of AZT. The expression of MRP4 could be successfully suppressed by *in vitro* and *in vivo* transfection of BCEC with anti-MRP4 pDNA producing siRNA. Using multifunctional peptide-PEG-conjugates and the biodegradable pLPEI polyplex in preparation of the systemic GDS, we demonstrated (a) an efficient accumulation of pDNA in BCEC of brain vasculature and (b) a high level of genetic inhibitor expression by pDNA delivered in the BBB. Our brain-targeted GDSs were able to diminish the activity of MRP4 DET following i.v. injections. We were able to abolish up to 60% of MRP4 activity. Evidently, the enhancement in AZT transport reached in our experiments can be additionally improved, for example, by using an efficient anti-MRP5 siRNA-producing vector. Some other transporters, like BCRP, were recently found to be active in the efflux of AZT from the BBB (36–38). All these facts may explain only a modest increase in the AZT permeability observed in this work. General applicability of RNA interference to the enhancement of chemotherapy complicated by the presence of DET has now been evaluated in multiple examples, mostly in the application to P-gp inhibition (39–41). The complexity and multifactorial nature of drug resistance was again demonstrated by some reported failures in the application of this approach (42). Nevertheless, our results give a positive proof-of-concept for this approach to be applied to the enhancement of chemotherapy of CNS-related diseases, and shed some light on directions for the improvement of systemic GDS.

CONCLUSION

We developed novel efficient transfection-enhancer molecules consisting of multifunctional peptides-PEG-*tris*-Acr intercalating conjugates for direct modification of plasmid DNA and a simple systemic brain-targeted GDS for the transfection of the BBB. At an optimal composition of these peptide conjugates in biodegradable polyplexes, the transfection of slow-dividing BCEC could be enhanced by nearly three orders of magnitude compared to naked pDNA. The new brain-targeted GDS demonstrated a high efficacy of *in vivo* delivery of anti-MRP4 pDNA into BCEC and an eventual down-regulation of the DET, resulting in a more than three-fold increase of AZT transport into the brain.

Acknowledgments

This work was supported by NIH grants NS050660 and NS063879 (S.V.V.). Authors are grateful to Mrs. Huai-Yun Han, Arin Zeman, and Galya Warren for excellent technical help in conducting some experiments. The assistance of UNMC Confocal Microscopy and Protein Analysis Core facilities is greatly appreciated.

ABBREVIATIONS

Acr	acridine
ApoE	Apolipoprotein E-derived peptide
BBB	blood-brain barrier
BCEC	brain capillary endothelial cells
BH	brain-homing peptide

BSA	bovine serum albumin
DAB	Diaminobenzidine
DET	drug efflux transporters
DLS	dynamic light scattering
ECL	chemoluminescence detection kit
GDS	gene delivery system
GFP	green fluorescent protein
HAART	highly active antiretroviral therapy
HPLC	high performance liquid chromatography
LPEI	linear polyethylenimine
NLS	SV40 nuclear localization signal peptide
NRTI	Nucleoside reverse transcriptase inhibitors
PAGE	Polyacrylamide gel electrophoresis
PEG	Poly(ethylene glycol)
TAT	HIV-1 trans-activator of transcription peptide

REFERENCES

1. Wagner E. Strategies to improve DNA polyplexes for *in vivo* gene transfer: will “artificial viruses” be the answer? Pharm Res 2004;21:8–14. [PubMed: 14984252]
2. Bremner KH, Seymour LW, Logan A, Read ML. Factors influencing the ability of nuclear localization sequence peptides to enhance nonviral gene delivery. Bioconjug Chem 2004;15:152–61. [PubMed: 14733595]
3. Escriou V, Carriere M, Scherman D, Wils P. NLS bioconjugates for targeting therapeutic genes to the nucleus. Adv Drug Deliv Rev 2003;55:295–306. [PubMed: 12564982]
4. Wadia JS, Dowdy SF. Transmembrane delivery of protein and peptide drugs by TAT-mediated transduction in the treatment of cancer. Adv Drug Deliv Rev 2005;57:579–96. [PubMed: 15722165]
5. Vendeville A, Rayne F, Bonhoure A, Bettache N, Montcourrier P, Beaumelle B. HIV-1 Tat enters T cells using coated pits before translocating from acidified endosomes and eliciting biological responses. Mol Biol Cell 2004;15:2347–60. [PubMed: 15020715]
6. Oupicky D, Ogris M, Seymour LW. Development of long-circulating polyelectrolyte complexes for systemic delivery of genes. J Drug Target 2002;10:93–8. [PubMed: 12074545]
7. Gilmore JL, Yi X, Quan L, Kabanov AV. Novel nanomaterials for clinical neuroscience. J Neuroimmune Pharmacol 2008;3:83–94. [PubMed: 18210200]
8. Loscher W, Potschka H. Drug resistance in brain diseases and the role of drug efflux transporters. Nat Rev Neurosci 2005;6:591–602. [PubMed: 16025095]
9. Kabanov AV, Batrakova EV. New technologies for drug delivery across the blood brain barrier. Curr Pharm Des 2004;10:1355–63. [PubMed: 15134486]
10. Boado RJ. Blood-brain barrier transport of non-viral gene and RNAi therapeutics. Pharm Res 2007;24:1772–87. [PubMed: 17554608]
11. Zhang H, Mitin A, Vinogradov SV. Efficient transfection of blood-brain barrier endothelial cells by lipoplexes and polyplexes in the presence of nuclear targeting NLS-PEG-acridine conjugates. Bioconjug Chem 2009;20:120–8. [PubMed: 19067581]
12. Zhang H, Vinogradov SV. Short biodegradable polyamines for gene delivery and transfection of brain capillary endothelial cells. J Control Release 2010;143:359–66. [PubMed: 20093156]

13. Chen Z, Varney ML, Backora MW, Cowan K, Solheim JC, Talmadge JE, Singh RK. Down-regulation of vascular endothelial cell growth factor-C expression using small interfering RNA vectors in mammary tumors inhibits tumor lymphangiogenesis and spontaneous metastasis and enhances survival. Cancer Res 2005;65:9004–11. [PubMed: 16204074]
14. Torchilin VP. Tatp-mediated intracellular delivery of pharmaceutical nanocarriers. Biochem Soc Trans 2007;35:816–20. [PubMed: 17635155]
15. Tiera MJ, Winnik FO, Fernandes JC. Synthetic and natural polycations for gene therapy: state of the art and new perspectives. Curr Gene Ther 2006;6:59–71. [PubMed: 16475946]
16. Lechardeur D, Lukacs GL. Nucleocytoplasmic transport of plasmid DNA: a perilous journey from the cytoplasm to the nucleus. Hum Gene Ther 2006;17:882–9. [PubMed: 16972756]
17. Nguyen J, Xie X, Neu M, Dumitrascu R, Reul R, Sitterberg J, et al. Effects of cell-penetrating peptides and pegylation on transfection efficiency of polyethylenimine in mouse lungs. J Gene Med 2008;10:1236–46. [PubMed: 18780309]
18. Deeva EG, Pavlovskaia V, Kiselev OI, Kiselev VI, Piotrovskii LB, Ershov FI. [The structural and functional analysis of the biological activity of acridine derivatives]. Vestn Ross Acad Med Nauk 2004:29–34.
19. Lechardeur D, Verkman AS, Lukacs GL. Intracellular routing of plasmid DNA during non-viral gene transfer. Adv Drug Deliv Rev 2005;57:755–67. [PubMed: 15757759]
20. Kloeckner J, Boeckle S, Persson D, Roedl W, Ogris M, Berg K, et al. DNA polyplexes based on degradable oligoethylenimine-derivatives: combination with EGF receptor targeting and endosomal release functions. J Control Release 2006;116:115–22. [PubMed: 16959361]
21. Ou M, Wang XL, Xu R, Chang CW, Bull DA, Kim SW. Novel biodegradable poly(disulfide amine)s for gene delivery with high efficiency and low cytotoxicity. Bioconjug Chem 2008;19:626–33. [PubMed: 18314939]
22. Bolhassani A, Ghasemi N, Servis C, Taghikhani M, Rafati S. The efficiency of a novel delivery system (PEI600-Tat) in development of potent DNA vaccine using HPV16 E7 as a model antigen. Drug Deliv 2009;16:196–204. [PubMed: 19514980]
23. Moore NM, Clayton CL, Sakiyama-Elbert SE. Characterization of multifunctional PEG-based gene delivery system containing nuclear localization signals and endosome escape peptides. Acta Biomater 2009;5:854–64. [PubMed: 18926782]
24. Nitin N, LaConte L, Rhee W-J, Bao G. TAT peptide is capable of importing large nanoparticles across nuclear membrane in digitonin permeabilized cells. Ann Biomed Engin 2009;37:2018–27.
25. Sadanandam A, Varney ML, Kinarsky L, Ali H, Mosley RL, Singh RK. Identification of functional cell adhesion molecules with a potential role in metastasis by a combination of *in vivo* phage display and *in silico* analysis. OMICS 2007;11:41–57. [PubMed: 17411395]
26. Takae S, Miyata K, Oba M, Ishii T, Nishiyama N, Itaka K, et al. PEG-detachable polyplex micelles based on disulfide-linked block catiomers as bioresponsive nonviral gene vectors. J Am Chem Soc 2008;130:6001–9. [PubMed: 18396871]
27. Kaleand AA, Torchilin VP. Enhanced transfection of tumor cells *in vivo* using “Smart” pH-sensitive TAT-modified pegylated liposomes. J Drug Target 2007;15:538–45. [PubMed: 17671900]
28. Wan L, Pooyan S, Hu P, Leibowitz MJ, Stein S, Sinko PJ. Peritoneal macrophage uptake, pharmacokinetics and biodistribution of macrophage-targeted PEG-fMLF (N-formyl-methionylleucyl-phenylalanine) nanocarriers for improving HIV drug delivery. Pharm Res 2007;24:2110–9. [PubMed: 17701325]
29. Romberg B, Hennink WE, Storm G. Sheddable coatings for long-circulating nanoparticles. Pharm Res 2008;25:55–71. [PubMed: 17551809]
30. Dallas S, Miller DS, Bendayan R. Multidrug resistance-associated proteins: expression and function in the central nervous system. Pharmacol Rev 2006;58:140–61. [PubMed: 16714484]
31. Zhou SF, Wang LL, Di YM, Xue CC, Duan W, Li CG, et al. Substrates and inhibitors of human multidrug resistance associated proteins and the implications in drug development. Curr Med Chem 2008;15:1981–2039. [PubMed: 18691054]

32. Labialle S, Dayan G, Michaud M, Barakat S, Rigal D, Baggetto LG. Gene therapy of the typical multidrug resistance phenotype of cancers: a new hope? Semin Oncol 2005;32:583–90. [PubMed: 16338424]
33. Wu CP, Calcagno AM, Ambudkar SV. Reversal of ABC drug transporter-mediated multidrug resistance in cancer cells: evaluation of current strategies. Curr Mol Pharmacol 2008;1:93–105. [PubMed: 19079736]
34. Galinsky RE, Hoesterey BL, Anderson BD. Brain and cerebrospinal fluid uptake of zidovudine (AZT) in rats after intravenous injection. Life Sci 1990;47:781–8. [PubMed: 2215081]
35. Jorajuria S, Dereuddre-Bosquet N, Becher F, Martin S, Porcheray F, Garrigues A, et al. ATP binding cassette multidrug transporters limit the anti-HIV activity of zidovudine and indinavir in infected human macrophages. Antivir Ther 2004;9:519–28. [PubMed: 15456083]
36. Giri N, Shaik N, Pan G, Terasaki T, Mukai C, Kitagaki S, et al. Investigation of the role of breast cancer resistance protein (Bcrp/Abcg2) on pharmacokinetics and central nervous system penetration of abacavir and zidovudine in the mouse. Drug Metab Dispos 2008;36:1476–84. [PubMed: 18443033]
37. Pan G, Giri N, Elmquist WF. Abcg2/Bcrp1 mediates the polarized transport of antiretroviral nucleosides abacavir and zidovudine. Drug Metab Dispos 2007;35:1165–73. [PubMed: 17437964]
38. Wangand X, Baba M. The role of breast cancer resistance protein (BCRP/ABCG2) in cellular resistance to HIV-1 nucleoside reverse transcriptase inhibitors. Antivir Chem Chemother 2005;16:213–6. [PubMed: 16130519]
39. Wu H, Hait WN, Yang JM. Small interfering RNA-induced suppression of MDR1 (P-glycoprotein) restores sensitivity to multidrug-resistant cancer cells. Cancer Res 2003;63:1515–9. [PubMed: 12670898]
40. Gan HZ, Zhang GZ, Zhao JS, Zhang FC, Bu LS, Yang SJ, et al. Reversal of MDR1 gene-dependent multidrug resistance using short hairpin RNA expression vectors. Chin Med J (Engl) 2005;118:893–902. [PubMed: 15978189]
41. Kaszubiak A, Holm PS, Lage H. Overcoming the classical multidrug resistance phenotype by adenoviral delivery of anti-MDR1 short hairpin RNAs and ribozymes. Int J Oncol 2007;31:419–30. [PubMed: 17611700]
42. Su Y, Lee SH, Sinko PJ. Inhibition of efflux transporter ABCG2/BCRP does not restore mitoxantrone sensitivity in irinotecan-selected human leukemia CPT-K5 cells: evidence for multifactorial multidrug resistance. Eur J Pharm Sci 2006;29:102–10. [PubMed: 16844360]

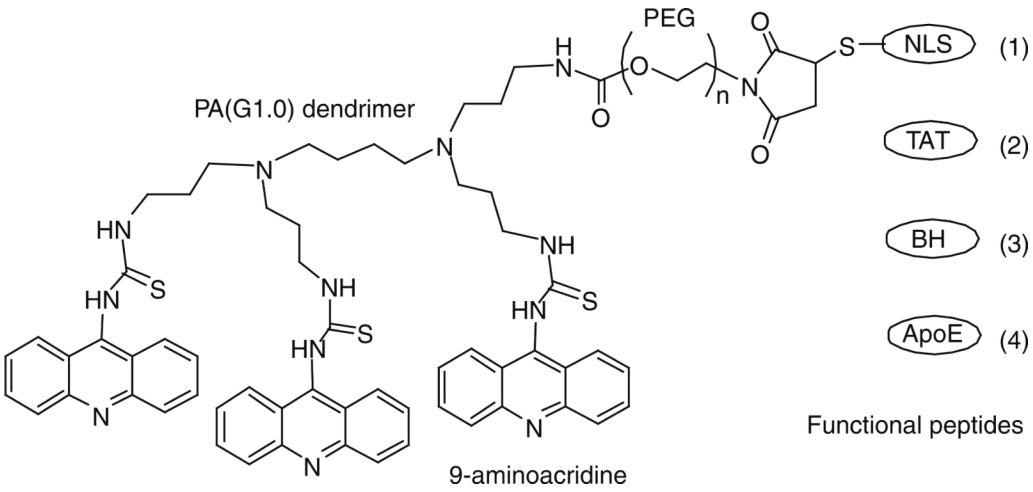

Fig. 1.
Chemical structure of peptide-PEG-*tris*-Acr conjugates.

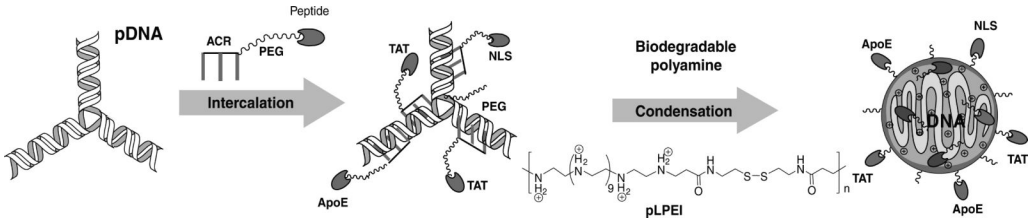

Fig. 2.

Preparation of core-shell polyplexes by direct binding of pDNA with peptide-PEG-*tris*-Acr conjugates and compacting of these intercalating complexes by short biodegradable pLPEI polyamines.

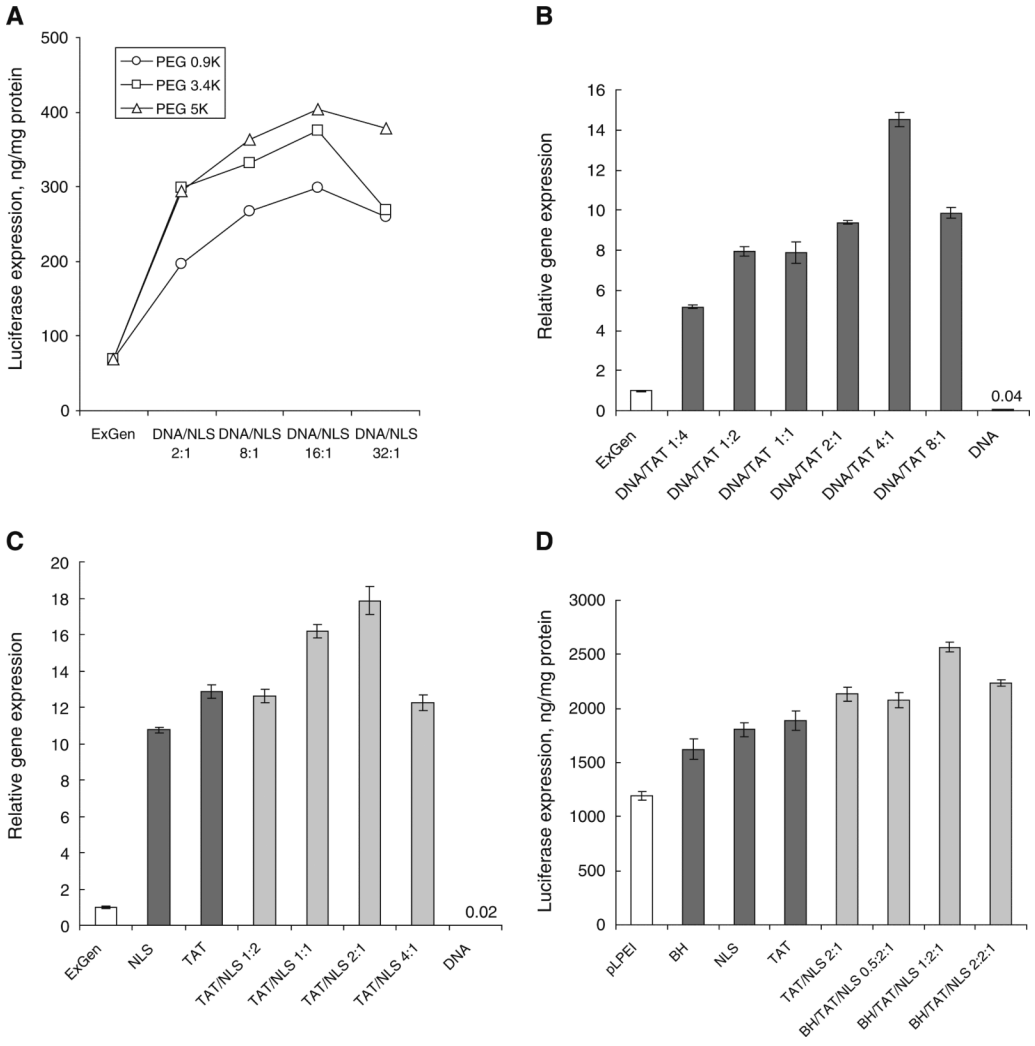

Fig. 3.

Optimization of the peptide-PEG-tris-Acr conjugate-mediated transfection of bEnd.3 cells. Standard transfection conditions were as follows: 0.5 μg luciferase-encoding pDNA per well, 4 h incubation with cells in the presence of 10% FBS, then expression analysis 48 h later (in quadruplicates; shown are means±SEM). (**A**) Effect of the PEG M.w. in NLS-PEG-*tris*-Acr conjugates on ExGen500-mediated transfection (N/P ratio 6). (**B**) Optimization of the TAT-PEG-*tris*-Acr content in ExGen500-polyplexes. (**C**) Optimization of the TAT/NLS-conjugates ratio in ExGen500 polyplexes. ExGen500 alone was used as a positive control, and its transfection level was taken for 1 in panes B and C. (**D**) Optimization of BH-PEG-tris-Acr content in pLPEI-polyplexes (N/P ratio 15). The pDNA/conjugates wt ratio was equal to 4 in panes C and D.

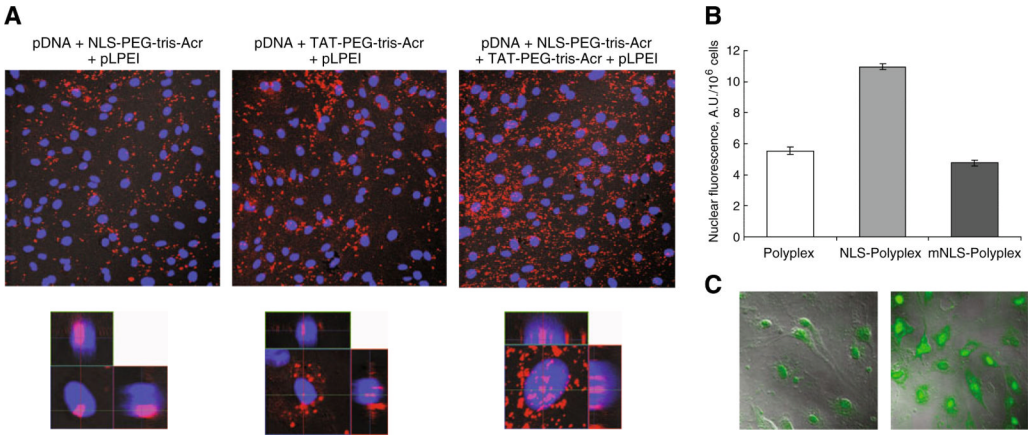

Fig. 4.

Internalization and nuclear accumulation of pDNA in bEnd3 cells. (**A**) Synergistic effect of NLS and TAT-conjugates on cellular trafficking of rhodamine-labeled pDNA compacted by pLPEI at N/P ratio 15. Confocal microscopy images are shown in normal (*upper panes*) and lateral modes (*lower panes*). Red color: pDNA, blue color: nuclei stained with DAPI. (**B**) Nuclear accumulation of rhodamine-labeled pDNA depending on effects of NLS or mutant NLS (mNLS)-conjugates (ExGen500-polyplexes). (**C**) Synergistic effect of two peptide-conjugates on the expression of GFP pDNA. Confocal images of NLS (*left*) and NLS+ApoE (1:1, *right*) conjugates were obtained 16 h post-transfection IExGen500-polyplexes).

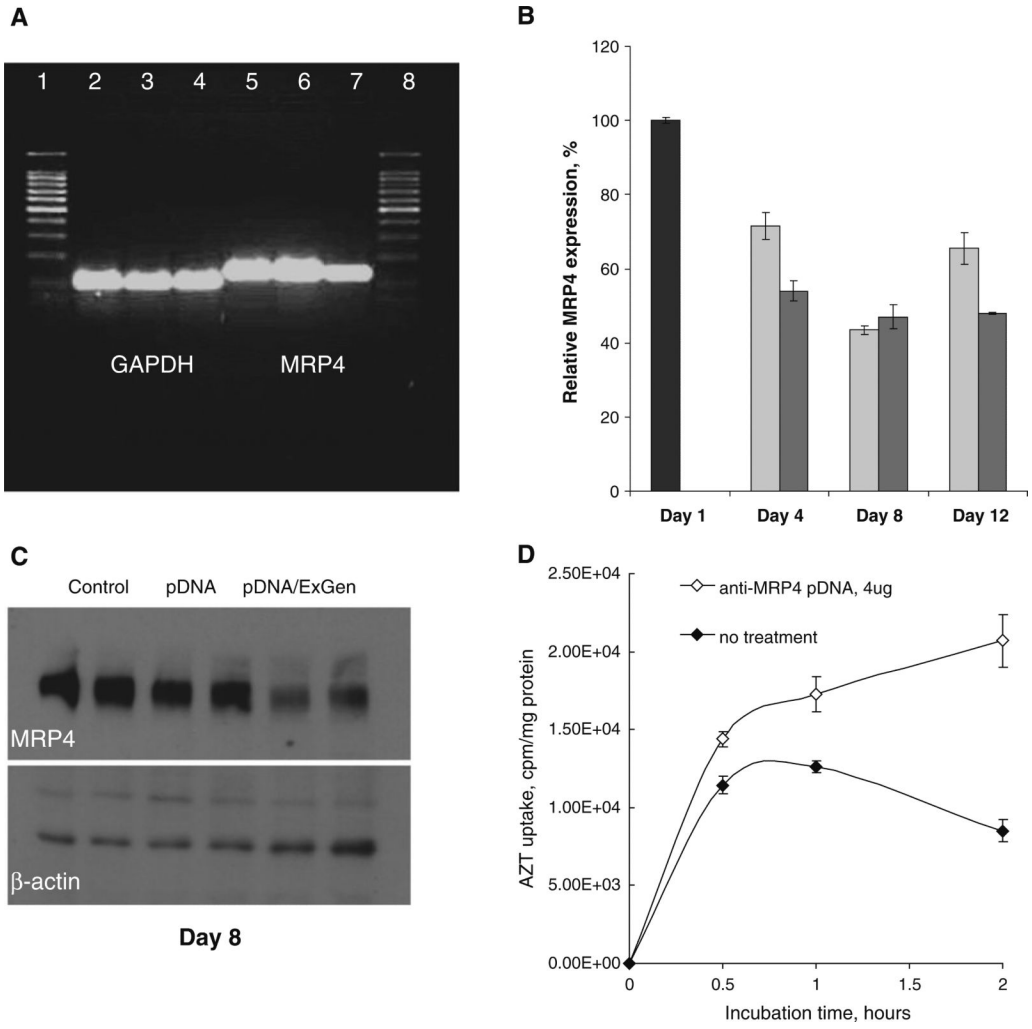

Fig. 5.

Down-regulation of MRP4 drug efflux transporter in bEnd3 cells by anti-MRP4 pDNA. (**A**) Agarose gel electrophoresis of DNA fragments following the real-time PCR analysis of GAPDH (lines 2–4) and MRP4 (lines 5–7) expression before (lines 2, 5: cell passage 23, lines 3, 6: cell passage 32), and after the treatment with anti-MRP4 pDNA (ExGen500 polyplexes) 48 h post-transfection (lines 4, 7). Lines 1 and 8: 100-bp DNA ladder. (**B**) Quantitative real-time PCR analysis of MRP4 mRNA expression on Days 4, 8 and 12 post-transfection with 2 μg(*light bars*), or 4 μg(*shaded bars*) of anti-MRP4 pDNA per 5×10^4 cells. Cells were treated with ExGen500 polyplexes for 4 h at 37°C in the presence of 10% FBS. The level of MRP4 mRNA expression in non-treated bEnd3 cells (Day 1) was taken for 100% (*darker bar*). (**C**) Western blotting analysis of the MRP4 protein expression on Day 8 post-transfection with anti-MRP4 pDNA (4 μg) in the presence of ExGen500 (in duplicates). Controls: non-treated cells and cells treated with pDNA without ExGen500. (**D**) Increase in the ^{3}H-AZT accumulation on Day 8 post-transfection with anti-MRP4 pDNA (4 μg) in the presence of ExGen500.

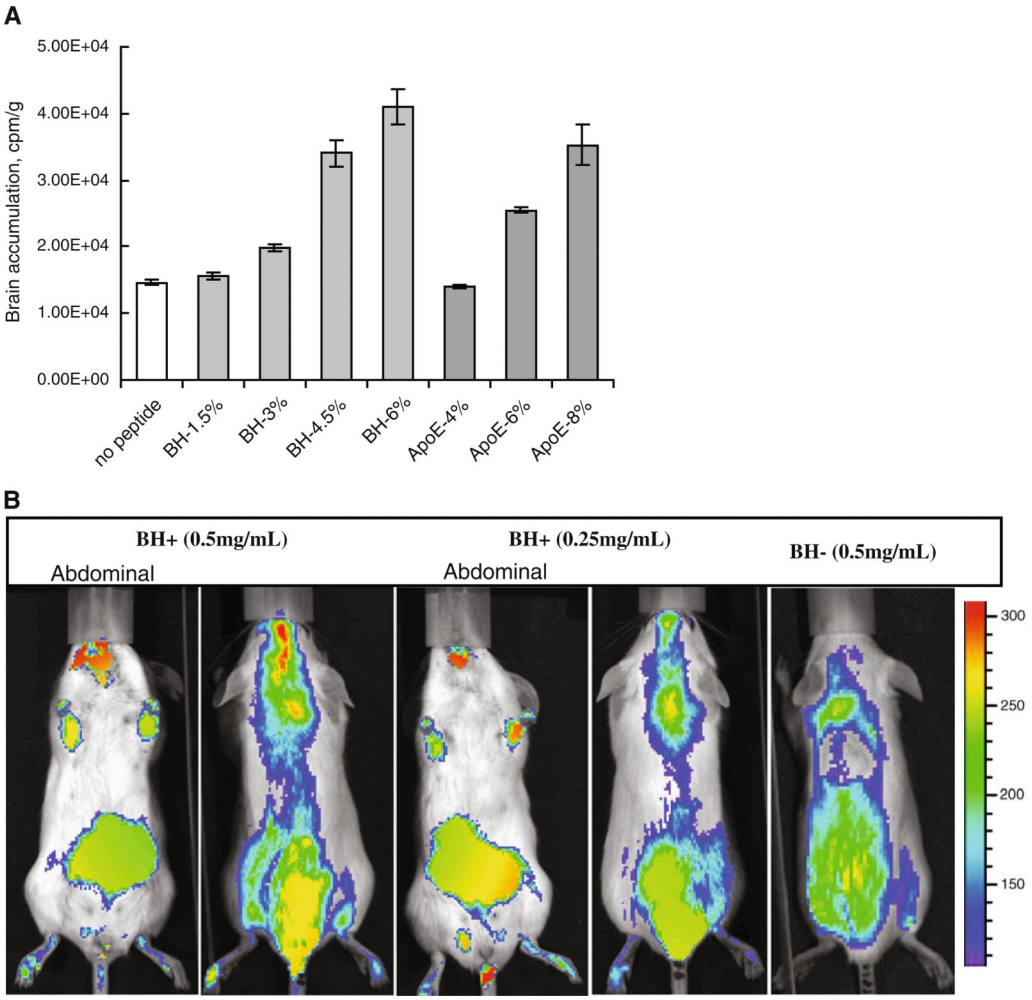

Fig. 6.

Brain accumulation and biodistribution of pDNA polyplexes in mice. (**A**) Brain accumulation of radiolabeled BH and ApoE-vectorized polyplexes (^{3}H-pLPEI) at different peptide contents (%wt); 1 h after i.v. injection in mice (n = 3). (**B**) Bioimaging of BH peptide-vectorized and non-vectorized pLPEI-polyplexes of rhodamine-labeled pDNA. Pictures were taken 1 h-post-injection in the tail vein of Balb/c mice using Xenogen IVIS-200 bioimager, and fluorescence intensities were converted by the instrument software.

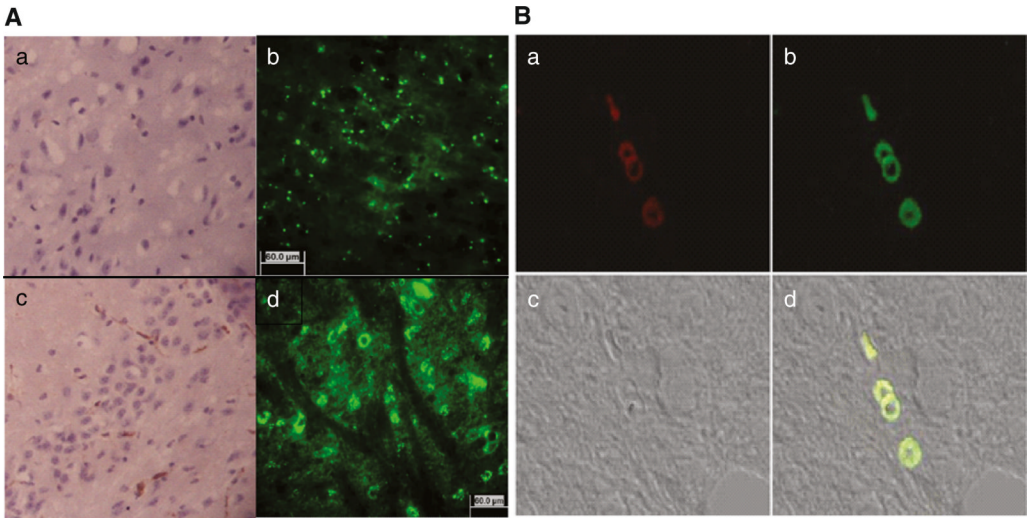

Fig. 7.

Vascular localization of GFP-expressing pDNA in mouse brain after i.v. administration. (**A**) anti-GFP mAb-HRP/DAB staining, and GFP fluorescence (*b*, *d*) in brain sections. a, b—non-vectorized nanoformulation, and c, d—brain-targeted ApoE-nanoformulation 48 h after i.v. injection of Balc/c mouse. (**B**) anti-CD34 mAb-Cy5 staining (*a*), GFP pDNA expression (*b*), bright field (*c*), and co-localization of the endothelial marker with GFP (*d*) in brain sections.

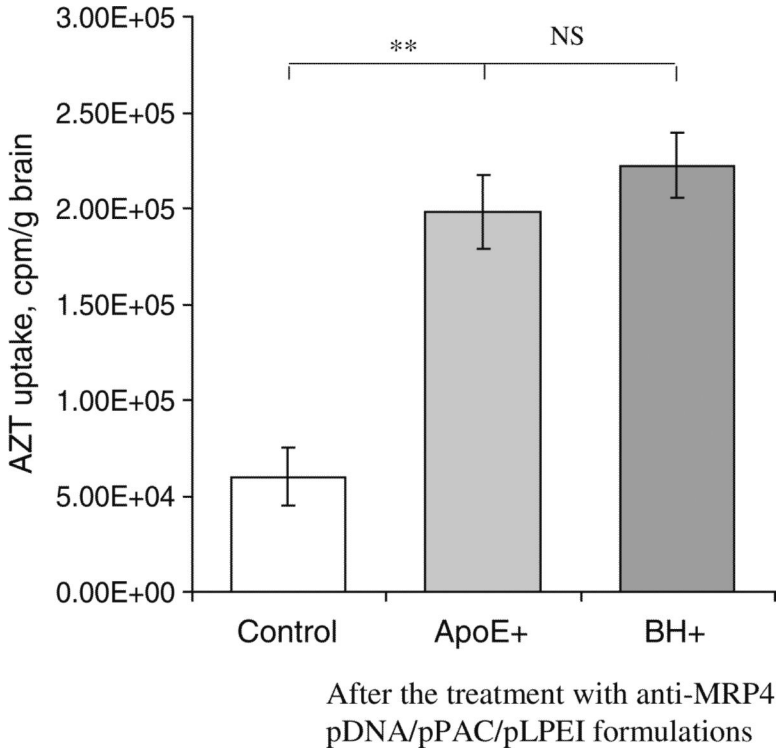

Fig. 8.

Effect of down-regulation of MPR4 DETon permeability of the BBB for drugs. ^{3}H-AZT accumulation in perfused brains was measured 4 h following an i.p. injection of mice on Day 9. Animals were treated on Days 1, 3 and 5 with 50 μg of anti-MRP4 pDNA/pPAC/pLPEI polyplex (n=4–5).

Table 1

Analytical Characteristics of Peptide-PEG_{5000}-*tris*-Acr Conjugates

Peptide conjugates	M.w. conjugate (peptide[1])	Acridine content, μmol/mg[2]	Peptide content, % (teor.)[3]	Aminoacid ratio[3]
NLS-PEG-*tris*-Acr	7,150 (1,127)	0.47	7.7 (15.8)	P1, K3.96, A1.96, V1.15, R1.06
TAT-PEG-*tris*-Acr	7,680 (1,662)	0.40	9.6 (21.6)	G1, K1.84, R5.66, Y1.2, Q0.93
BH-PEG-*tris*-Acr	6,950 (928)	0.44	6.3 (13.4)	A1, N + D1.97, F1.27, T1.12, P1.06, Y1.16
ApoE-PEG-*tris*-Acr	7,570 (1,548)	0.39	9.3 (20.4)	G1, R3.93, K1.93, L3.96

[1] Peptide M.w. values are based on mass-spectrometry data

[2] Determined by UV-spectrophotometry in aqueous solution of 1 mg/mL (ε_{420} 5,500)

[3] Calculated based on the aminoacid content after acidic hydrolysis; cystein was largely degraded, so the peptide content may be slightly underestimated